Gyrokinetic studies of core turbulence features in ASDEX Upgrade H-mode plasmas

A. Bañón Navarro,[1,2,a)] T. Happel,[1] T. Görler,[1] F. Jenko,[1,2,3] J. Abiteboul,[1] A. Bustos,[1] H. Doerk,[1] D. Told,[1,2] and the ASDEX Upgrade Team[1]

[1)]*Max-Planck-Institut für Plasmaphysik, Boltzmannstrase 2, 85748 Garching, Germany*

[2)]*Department of Physics and Astronomy, University of California, Los Angeles, California 90095, USA*

[3)]*Max-Planck/Princeton Center for Plasma Physics*

(Dated: 25 January 2017)

Gyrokinetic validation studies are crucial for developing confidence in the model incorporated in numerical simulations and thus improving their predictive capabilities. As one step in this direction, we simulate an ASDEX Upgrade discharge with the GENE code, and analyze various fluctuating quantities and compare them to experimental measurements. The approach taken is the following. First, linear simulations are performed in order to determine the turbulence regime. Second, the heat fluxes in nonlinear simulations are matched to experimental fluxes by varying the logarithmic ion temperature gradient within the expected experimental error bars. Finally, the dependence of various quantities with respect to the ion temperature gradient is analyzed in detail. It is found that density and temperature fluctuations can vary significantly with small changes in this parameter, thus making comparisons with experiments very sensitive to uncertainties in the experimental profiles. However, cross-phases are more robust, indicating that they are better observables for comparisons between gyrokinetic simulations and experimental measurements.

I. INTRODUCTION

It has been known for several decades that energy and particle confinement in tokamak plasmas are mainly degraded by turbulence driven by steep temperature and density gradients. For this reason, the characterization and understanding of these turbulent processes is a very important task in order to improve the performance of present experiments as well as future fusion reactors.

Due to the strong background magnetic field and the low collisionality in tokamak plasmas, gyrokinetic theory has been established as the most appropriate theoretical framework for the study of turbulent transport in the plasma core. In order to improve confidence in the numerical results obtained with gyrokinetics and to establish a solid understanding of turbulent transport across the whole range of plasma parameters, it is very important to perform direct comparisons between simulations and experimental measurements. In this respect, with the recent development and improvements in fluctuations diagnostic, it is now possible to measure turbulence features with high precision, allowing for quantitative comparisons between experimental data and results of nonlinear gyrokinetic simulations. These validation studies are crucial in developing confidence in the models and improving the predictive capabilities of the numerical simulations. For these reasons, experiments and gyrokinetic codes from across the world are focused on this goal. The work performed for DIII-D[1–6], Alcator C-Mod[7], TORE Supra[8], and FT-2[9] discharges are examples of such efforts.

In a recent paper[10], we have compared density fluctuation levels measured with a new Doppler reflectometer installed in ASDEX Upgrade and simulation results obtained with the gyrokinetic GENE code. We extend the previous work by additionally presenting simulation results of density wavenumber spectra, electron temperature fluctuation levels as well as cross-phases between different quantities. One of the reasons for analyzing electron temperature fluctuation levels and cross-phases is that a new Correlation Electron Cyclotron Emission (CECE) system is expected to be installed and to be in operation in 2015 in ASDEX Upgrade. Therefore, the gyrokinetic results presented in this paper can provide guidance for the on-going development of the diagnostic. From a more fundamental point of view, we will also investigate the variation of these quantities with respect to various physical input parameters. This information can be used to characterize core turbulence features in ASDEX Upgrade plasmas.

The paper is organized as follows. In Section II, an overview of the chosen plasma discharge analyzed is given. A description of the gyrokinetic simulation method used is described in Section III. Micro-instability studies from linear gyrokinetic simulations are outlined in Section IV. The main results of the paper are shown in Section V. Core turbulence features such as heat fluxes, density fluctuation amplitudes and spectra, temperature fluctuation amplitudes as well as cross-phases between these quantities will be presented in detail, followed by a discussion in Section VI. Finally, conclusions and future work will be discussed in Section VII.

II. OVERVIEW OF THE PLASMA DISCHARGE

The ASDEX Upgrade discharge #28245 analyzed in this paper was operated in the high-confinement regime (H-mode). It was planned to study the turbulence characteristics in both the ion temperature gradient (ITG) and trapped electron mode (TEM) regimes, through a transition from one regime to another. This transition can be achieved by modifying locally the electron temperature gradient, which affects the TEM instabil-

[a)]Electronic mail: banon@physics.ucla.edu

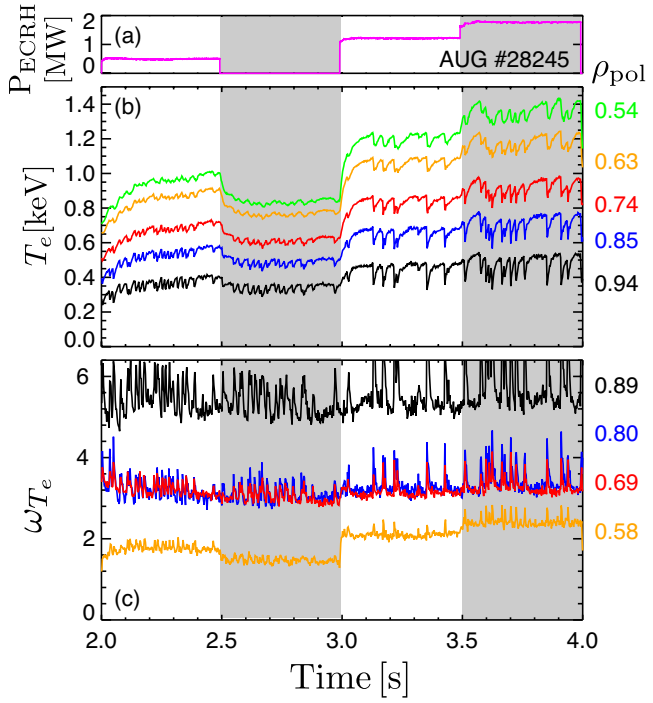

FIG. 1. (color online) Time traces of ASDEX Upgrade discharge #28245. (a) ECRH heating power, (b) electron temperature and (c) logarithmic electron temperature gradient at different radial positions. The data is analyzed in the time intervals shaded in grey.

ity. This is obtained by changing the electron cyclotron resonance heating power (ECRH) by steps during the discharge.

In this discharge, neutral beam injection with heating power of 2.5 MW is used throughout the discharge to obtain a steady state H-mode plasma. The magnetic field strength on axis is $B = 2.27$ T and the plasma current $I_p = 600$ kA. An overview of several relevant time traces is given in Fig. 1. The ECRH power $P_{\rm ECRH}$ is deposited at $\rho_{\rm pol} = 0.5$ from $2.0-4.0$ seconds. Here, $\rho_{\rm pol}$ is the normalized poloidal flux radius. At this heating location, $P_{\rm ECRH}$ is varied subsequently between $0.5, 0.0, 1.2$ and $1.8\,$MW (a). The influence of the stepped heating power can be clearly observed in the electron temperature T_e (b). Finally, the strongest increase of the logarithmic temperature gradient ω_{T_e} is observed at $\rho_{\rm pol} \approx 0.6$ when an ECRH power of 1.8 MW is applied (c). For this reason, this case and the one without ECRH will be analyzed in detail, as examples of the two extreme cases. They correspond to the time windows shaded in grey in Fig. 1. Within these time windows, we have simulated three different radial locations: $\rho_{\rm pol} = \{0.6, 0.7, 0.8\}$, making a total of six different scenarios to be studied with gyrokinetic simulations.

The physical parameters for each of these six cases are given in Table I. There, the reference length is defined as $L_{\rm ref} = \sqrt{\Psi_{\rm tor,sep}/\pi B_{\rm ref}}$, where $\Psi_{\rm tor,sep}$ is the toroidal flux at the separatrix and $B_{\rm ref}$ is the magnetic field on axis. Typically, this reference length is comparable but not identical to the tokamak minor radius. The logarithmic gradients are defined as in Ref. 11: $\omega_X = -\frac{1}{X}\frac{{\rm d}X}{{\rm d}\rho_{\rm tor}}$ with $X \in \{T_i, T_e, n_e\}$, and $\rho_{\rm tor}$ the normalized toroidal flux radius. The magnetic shear is given as $\hat{s} = \frac{\rho_{\rm tor}}{q}\frac{{\rm d}q}{{\rm d}\rho_{\rm tor}}$, where q is the safety factor, and the electron beta is defined as $\beta_e = 2\mu_0 n_e T_e / B^2_{\rm ref}$. Here, T_i and T_e are the ion and electron temperature, respectively, and n_e is the electron density. The electron-ion collision frequency ν_{ei} is defined as in Ref. 12. The $E \times B$ shear rate is defined as $\gamma_E = -\rho_{\rm tor}/q\,(\partial\omega_t/\partial\rho_{\rm tor})$, with $\omega_{\rm t}$ the toroidal rotation frequency. Finally, $Z_{\rm eff}$ is the effective charge calculated taken into account boron density measurements with a charge exchange recombination spectroscopy (CXRS). For more details on the discharge parameters, see Ref. 10.

Time [s]	2.65-2.95	2.65-2.95	2.65-2.95	3.65-3.95	3.65-3.95	3.65-3.95
I_p [kA]	600	600	600	600	600	600
$\rho_{\rm pol}$	0.60	0.70	0.80	0.60	0.70	0.80
$\rho_{\rm tor}$	0.47	0.56	0.67	0.47	0.56	0.67
$\hat{s}$	0.73	1.05	1.47	0.59	1.00	1.63
q	2.39	2.82	3.56	2.22	2.57	3.24
ω_{T_i}	1.69	2.05	2.01	1.10	1.49	2.06
ω_{T_e}	1.44	2.06	1.82	2.15	2.11	2.16
ω_{n_e}	0.01	0.24	0.48	0.59	0.43	0.49
β_e [%]	0.29	0.24	0.19	0.50	0.39	0.29
T_i [keV]	0.77	0.64	0.50	0.86	0.76	0.64
T_e [keV]	0.80	0.68	0.54	1.23	1.00	0.80
n_e [10^{19} m^{-3}]	4.40	4.36	4.25	4.83	4.63	4.39
$Z_{\rm eff}$	1.16	1.16	1.16	1.14	1.15	1.16
$\nu_{ei}[L_{\rm ref}/c_s]$	0.39	0.52	0.74	0.18	0.25	0.38
$\gamma_E[L_{\rm ref}/c_s]$	0.02	0.02	0.02	0.01	0.01	0.01
$R_{\rm axis}/L_{\rm ref}$	2.51	2.51	2.51	2.59	2.59	2.59
$B_{\rm ref}$ [T]	2.21	2.21	2.21	2.19	2.19	2.19
$L_{\rm ref}$ [m]	0.68	0.68	0.68	0.66	0.66	0.66
ρ_s [cm]	0.18	0.17	0.15	0.23	0.21	0.18

TABLE I. Physical parameters for the six simulated ASDEX Upgrade cases. $R_{\rm axis}$ is the major radius at the magnetic axis and $\rho_s = c_s/\Omega_i$ is a reference gyroradius defined with the ion sound speed $c_s = \sqrt{T_e/m_i}$ and the ion gyrofrequency Ω_i.

III. OVERVIEW OF THE GYROKINETIC SIMULATION METHOD

The turbulence data obtained in this paper are produced with the gyrokinetic code GENE, which solves self-consistently the gyrokinetic-Maxwell system of equations on a fixed grid in five dimensional phase space (plus time): two velocity coordinates $(v_\parallel, \mu)$ and three field-aligned coordinates (x, y, z). Here, z is the coordinate along the magnetic field line, while the radial coordinate x and the binormal coordinate y are orthogonal to the equilibrium magnetic field. The velocity coordinates are, respectively, the velocity parallel to the magnetic field and the magnetic moment. GENE has the possibility to simulate either a flux-tube (local simulations) or a full torus (global simulations). In the former option, it is assumed that the relevant turbulent structures are small with respect to the radial variation of the background profiles and gradients. This allows to use periodic boundary conditions and thus the coordinates perpendicular to the magnetic field are Fourier transformed $(x, y) \rightarrow (k_x, k_y)$. For this work,

only the local version of the code has been employed.

The GENE code is physically comprehensive and includes many features (see Ref. 13 for more details). For the ASDEX Upgrade scenario studied in this paper, the following features of the GENE code were used: two particle species (deuterons and electrons), electromagnetic effects by solving the parallel component of Ampère's law, external $E \times B$ shear, parallel flow shear and a linearized Landau-Boltzmann collision operator with energy and momentum conserving terms[14], which includes also the effective charge ($Z_{\rm eff}$) in order to mimic at least parts of the missing impurities in two kinetic species simulations. Unless stated otherwise, the magnetic equilibrium geometry is taken from the TRACER-EFIT interface[15]. Additionally, GyroLES techniques have been used to reduce the accumulation of energy at the smallest scales (see Refs. [16–18]). Further simulation details, such as resolution grid, box sizes, etc., are given in the following sections.

IV. MICRO-INSTABILITY STUDIES: LINEAR GYROKINETIC SIMULATIONS

In order to calculate turbulent transport fluxes, density and temperature fluctuation amplitudes, etc., nonlinear gyrokinetic simulations are necessary. Nevertheless, linear gyrokinetic simulations can provide useful insights. For instance, they may allow us to identify the underlying microinstabilities which drive the turbulence present in the experiments. They can also be used for convergence studies and, since they are usually computationally cheap, they can also be used to do scans in different physical parameters.

A. Nominal parameter set

In linear simulations we calculate the growth rate and frequency of the most unstable mode present in the system for a given binormal wave vector k_y and $k_x = 0$. In this paper we choose to present k_y in $\rm cm^{-1}$ instead of the more common $k_y\rho_s$ units. This has been done in order to compare to experimental results. For reference, ρ_s values are given in Table I.

In Fig 2, we display the growth rates (γ) and frequencies (ω) for the cases at $\rho_{\rm pol} = 0.6$, because similar conclusions are obtained at other radial positions. In the figure, the negative frequencies are represented by dashed lines. The grid resolution was $\{x, z, v_\parallel, \mu\} = \{31, 32, 48, 16\}$. Convergence tests were performed at higher resolutions and confirm the validity of the results. Several observations can be made. First, for low wavenumbers, ITG is the dominant instability. This is indicated by a positive frequency, which with the present normalization represents a frequency in the ion diamagnetic direction. Second, for all the cases analyzed, the TEM mode is stable (studied with an eigenvalue solver). It was shown in Ref. 10 that adding ECRH has the effect of approaching to a regime dominated by TEM, and that only with the combination of a much higher electron temperature gradient and a lower ion temperature gradient than the ones measured experimentally, do TEM modes become unstable[19]. Finally, for higher wavenumbers, ETG is the dominant instability (indicated by a negative frequency). The effect of ECRH is to increase the growth rates of ETG modes, possibly leading to a subsequent increase of the electron heat flux for these cases. However, based on the ratio between the maximum ETG and ITG growth rates (rule-of-thumb emerged from Refs. 20 and 21), for both cases we expect the ETG contribution to the electron heat flux to be small with respect to the ITG contribution. This ratio has been successfully applied in Refs. 22 and 23 to predict the contribution of ETG modes in the electron heat transport in nonlinear gyrokinetic simulations. Moreover, ETG modes are not expected to influence density and temperature fluctuations at low wavenumbers, which are dominated by ITG. Since these are the scales measured by the diagnostics we are considering here, in this work we will limit ourselves to wavenumbers up to $k_y = 10\,\rm cm^{-1}$, thus excluding ETG modes, but allowing for a significant reduction in computational resources.

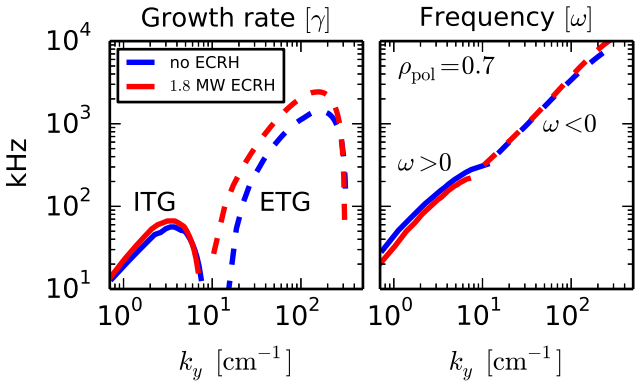

FIG. 2. (color online) Linear growth rates (left) and frequencies (right) for the cases at $\rho_{\rm pol=0.7}$ versus the binormal wavenumber k_y. The dashed lines in the figure indicate negative frequency values. Positive frequencies refer to modes drifting in the ion diamagnetic direction and negative in the electron diamagnetic direction. For these cases, they correspond to ITG and ETG modes, respectively.

B. Sensitivity studies with respect to the main physical parameters

Physical parameters such as temperature, density, magnetic equilibrium profiles, etc., are measured with experimental uncertainties. Since these values are used as input in the gyrokinetic codes, the uncertainty in these quantities could affect the simulation results. Therefore, sensitivity studies are carried out, with the aim of studying the effect of the different uncertainties on the simulation results. Ideally, these studies should be done in nonlinear gyrokinetic simulations. However, due to the expensive computational effort associated, this is in practice unfeasible. For this reason, this sensitivity study is done within linear gyrokinetic simulations.

We have studied the sensitivity of the linear growth rate with respect to a variation of $\pm 20\,\%$ in the nominal value for different physical parameters, such as: logarithmic ion

temperature gradient (ω_{T_i}), logarithmic electron temperature gradient (ω_{Te}), logarithmic electron density gradient (ω_{n_e}), electron to ion temperature ratio (T_e/T_i), collisionality ($\nu_{\rm col}$), safety factor (q) and magnetic shear ($\hat{s}$). At this point, we want to mention that the chosen sensitivity variation of ($\pm 20\,\%$) is based on an estimation of the uncertainties in the gradients[10], and it has not been rigorously estimated for the other parameters.

The main results are summarized in Table II. For simplicity, we show only cases at $\rho_{\rm pol} = 0.7$, although similar conclusions were obtained to the other radial positions. The sensitivity studies for q and for $\hat{s}$ have been done using a Miller-type magnetic equilibrium[24]. As is shown in Table II, the peak of the growth rates are practically insensitive with respect to changes of $\pm 20\%$ in ω_n, ω_{Te}, $\nu_{\rm col}$, q and $\hat{s}$. Changes in the peak of the growth rate up to $20\,\%$ are found for T_e/T_i variations. The most critical parameter is ω_{T_i}, whose $\pm 20\%$ variation modifies the growth rate by up to $40\,\%$ (see Fig. 3). Based on these results, one could expect that the uncertainties in ω_{T_i} will have the largest influence in nonlinear gyrokinetic simulations. For this reason, in the following, we will mainly focus on the influence of this parameter on nonlinear simulations. As mentioned previously, a local change of $\pm 20\%$ in ω_{T_i} can be justified, since it is compatible within the uncertainties in the measured ion temperature profiles with a CXRS, as it is shown in Figure 18 of Ref. 10 for the same discharge of this paper.

The influence of the $E\times B$ shear (γ_E) is in general expected to have also a relevant impact on the transport in nonlinear simulations. In particular, we found that for all the cases considered, $\gamma_E/\gamma_{\rm max} < 0.25$, with $\gamma_{\rm max}$ the maximum growth rate. However, it has been found that the effect is negligible in nonlinear simulations, since even an increase of 40 % in γ_E showed no significant impact the heat fluxes. Nevertheless, the effect of the $E\times B$ and parallel flow shears are included in all the nonlinear simulations presented in this paper. Finally, since it has been observed that dilution effect from impurities can impact the growth rates[3], test cases with Boron as the third kinetic species were run but gave only small differences with respect to the two species results (less than 10 % deviation in growth rates and heat fluxes).

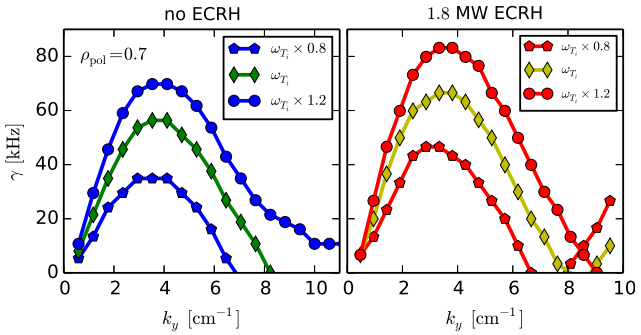

FIG. 3. (color online) Linear growth rates versus the binormal wavenumber k_y for the cases at $\rho_{\rm pol} = 0.7$ with respect to the variation of the logarithmic ion temperature gradient.

No ECRH	$\Delta\gamma$	1.8 MW ECRH	$\Delta\gamma$
$\omega_{Ti}\times 0.8$	-38 %	$\omega_{Ti}\times 0.8$	-30%
$\omega_{Ti}\times 1.2$	+25 %	$\omega_{Ti}\times 1.2$	+26%
$\omega_{T_e}\times 0.8$	-4 %	$\omega_{T_e}\times 0.8$	-5%
$\omega_{T_e}\times 1.2$	+5 %	$\omega_{T_e}\times 1.2$	+5%
$\omega_{n_e}\times 0.8$	+0 %	$\omega_{n_e}\times 0.8$	-5%
$\omega_{n_e}\times 1.2$	+0 %	$\omega_{n_e}\times 1.2$	+6 %
$T_e/T_i\times 0.8$	+14 %	$T_e/T_i\times 0.8$	+11 %
$T_e/T_i\times 1.2$	-18 %	$T_e/T_i\times 1.2$	-9%
$q\times 0.8$	-14 %	$q\times 0.8$	-9 %
$q\times 1.2$	+5 %	$q\times 1.2$	+6%
$\hat{s}\times 0.8$	+0 %	$\hat{s}\times 0.8$	-5%
$\hat{s}\times 1.2$	-4 %	$\hat{s}\times 1.2$	+5 %
$\nu_{\rm col}\times 0.8$	+5 %	$\nu_{\rm col}\times 0.8$	+6%
$\nu_{\rm col}\times 1.2$	-4 %	$\nu_{\rm col}\times 1.2$	-5 %

TABLE II. Percentage difference in maximum growth rate with respect to the nominal values for cases at $\rho_{\rm pol} = 0.7$ for various parameters (ω_{Ti}, ω_{Te}, ω_n, T_i/T_e, q, $\hat{s}$, and $\nu_{\rm col}$).

V. CORE TURBULENCE FEATURES: NONLINEAR GYROKINETIC SIMULATIONS

In order to predict and compare with experimental results, nonlinear simulations are required. For the selected discharge, the grid resolution needed is $\{256\times 128\times 32\times 48\times 16\}$ points in $\{x, y, z, v_\parallel, \mu\}$ coordinates. A convergence test of the results with that resolution has been performed by comparison with nonlinear simulations with a double resolution in the perpendicular directions for a few cases. Perpendicular box sizes of $125\,\rho_s$ units have been chosen in such a way that several correlation lengths fit in the box, and convergence checks have also been done in this respect to ensure the validity of this choice. Moreover, we have set the maximum wavenumber to $k_y \approx 10\,{\rm cm}^{-1}$. Results of the simulations are time-averaged over a range well exceeding the correlation time of the underlying turbulence (a range at least 400 $L_{\rm ref}/c_s$ units in the quasi-stationary state.)

A. Turbulence ion and electron heat fluxes

In this section, we compare the experimental ion and electron heat fluxes obtained through power balance analysis with the ASTRA[25] code and the results from nonlinear GENE simulations. As was done previously, we have grouped in the same plot the cases taken at the same radial position. The results are shown in Fig. 4.

Ion (electron) heat fluxes are shown in the left (right) columns in Fig. 4. The rows represent radial positions $\rho_{\rm pol} = 0.6, 0.7, 0.8$. The dashed lines indicate the ASTRA results and their shaded regions are used to indicate the uncertainty of the ASTRA values. Although for this discharge, we do not have a rigorous estimation of the uncertainty of the ASTRA results,

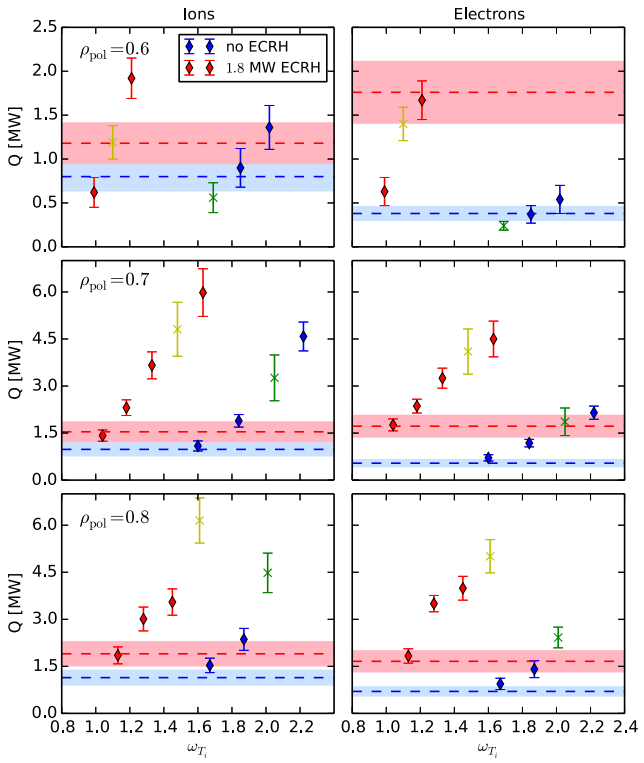

FIG. 4. (color online) Comparison of experimental heat fluxes (dashed-lines) with those obtained from gyrokinetic nonlinear GENE simulations (markers) using the nominal parameters and the variation with respect to logarithmic ion temperature gradient for all cases. Ion heat fluxes (left) and electron heat fluxes (right) are depicted. The rows represent the radial positions $\rho_{\rm pol} = 0.6, 0.7, 0.8$. The experimental values are obtained through power balance analysis with the ASTRA code and the shaded regions are used to indicate the uncertainty of the ASTRA values. In this case, a 20% error is assumed for all cases. In blue are the discharge parameters without ECRH heating and in red with ECRH heating. The nominal parameter in each case is colored differently to distinguish it from the rest.

a 20 % uncertainty has been chosen as an approximate value. Based on the linear sensitivity studies, for each case, several simulations were performed varying the logarithmic ion temperature gradient in steps of $\pm 10\%$ with respect to the nominal values, up to a maximum of $\pm 30\%$ variation. GENE simulation results are represented by the markers in the figure. The cases without ECRH are colored in blue and with ECRH in red and for each set, the simulations with the nominal parameters are colored differently (in green for the cases without ECRH and in yellow for the cases with ECRH). The statistical error bar is an estimation of the standard deviation of the set of means of consecutive temporal sub-domains of the saturated state. Several conclusions can be obtained from Fig. 4. For the nominal parameters, the cases with ECRH produce more ion and electron heat flux than the ones without ECRH for all positions. In addition, although not shown in the figure, the electromagnetic contribution to the heat flux is negligible (less than 5% of the total heat flux). For the case with ECRH heating at $\rho_{\rm pol} = 0.6$, the ion and electron heat fluxes match the experimental values without having to vary the gradient with respect to the nominal value. At this position, ω_{T_i} must be increased by 10% for the case without ECRH heating in order to match the experimental values. For the other positions, the values of the heat fluxes obtained with the nominal parameters clearly overestimate the heat fluxes obtained with ASTRA by a factor of $2-3$. We need to decrease ω_{T_i} by 20% in order to match the experimental results for the cases without ECRH. Whilst, for the cases with ECRH heating, it has to be decreased by a maximum of 30%. In Fig. 5, we summarize the modifications of the nominal logarithmic ion temperature gradient done in order to match the experimental heat fluxes. We can conclude that agreement of the transport levels within the errors bars can be achieved, since even small uncertainties in the temperature profile itself may translate to relatively large ones (up to $20-30\%$) in the logarithmic gradients[6,10].

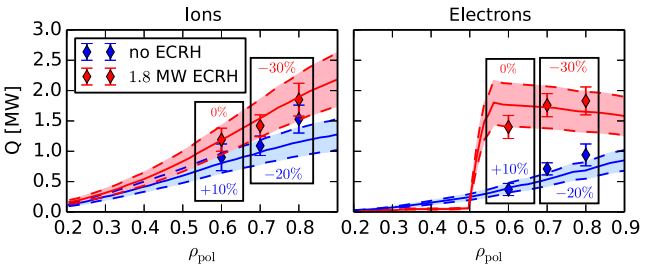

FIG. 5. (color online) Comparison of the experimental fluxes (dashed-lines) with those obtained from gyrokinetic nonlinear GENE simulations (markers) using the flux-matched simulations. The modifications of the nominal logarithmic ion temperature gradient done in the simulations in order to match the experimental fluxes is also indicated.

B. Turbulence electron density amplitudes

Since turbulent fluxes are caused by plasma fluctuations on microscopic scales, it is necessary to validate gyrokinetic codes on a microscopic level. In this regard, a new Doppler reflectometer has been recently installed in ASDEX Upgrade (see Ref 10 for more details on the diagnostic), which is able to measure electron density fluctuation amplitudes ($\tilde{n}_e$). In order to compare experimental and numerical results, a synthetic diagnostic must be implemented in GENE to reproduce the measurement process of the reflectometer. Two kinds of synthetic diagnostics can be employed. A first approach consists in simply filtering the data taking into account only the location and the wavenumbers that the diagnostic measures. This translates to take into account only fluctuations at the outboard mid-plane ($z = 0$), averaged over a finite radial length and then to select the range of perpendicular wavenumber that are measured in each case ($k_{y,\rm min}^{\rm measured} \leq k_y \leq k_{y,\rm max}^{\rm measured}$ in GENE). A more sophisticated method uses a full-wave code to simulate also the incidence and reflection of the wave into the gyrokinetic turbulent data[26]. This work is in progress and only preliminary results are available with this synthetic diagnostic (see Ref. 27). For this reason, we have only used the

filtering method for this work.

Comparison of the experimental and simulated $\tilde{n}_e$ are shown in Fig. 6. The simulations that match the experimental ion heat fluxes are shown with a different marker to distinguish them from the rest. The fluctuation data is analyzed considering only perpendicular wavenumbers between $4 \leq k_y \leq 8\,[\mathrm{cm}^{-1}]$. The experimental values are scaled by a common factor since the measurements are in arbitrary units. For this reason, only the shape of radial turbulence level profiles and the effect of ECRH can be used for comparison. We decided to scale the experimental values to try to match the case without ECRH. As is shown in the left plot of Fig. 6, we obtain a remarkable agreement between experimental and simulations results in the radial trend. For the case of 1.8 MW ECRH, there is also a good agreement in the turbulence level profile. However, with the scale used, the fluctuation levels are clearly underestimated with respect to the ones measured experimentally. In particular, the flux-matched results present the biggest discrepancy with respect to the experimental measurements. Finally, from this figure we can also observe how sensitive the density fluctuations are with respect to variations in the ion logarithmic temperature gradient. For instance, a 30% reduction in the logarithmic gradient can reduce density fluctuation levels by more than a factor of 2.

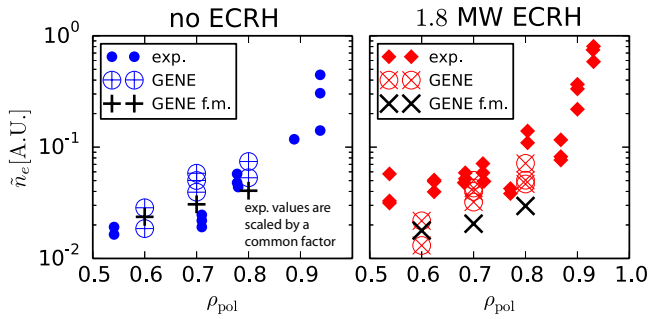

FIG. 6. (color online) Electron density fluctuation amplitudes at different radial positions. Blue-plus markers represent the data without ECRH heating, red-cross markers with ECRH and experimental results are in full circles. The flux-matched (GENE f.m.) simulations are marked differently. Fluctuation data is analyzed at the outboard mid-plane, averaged over a finite radial length and with perpendicular wavenumbers between $4 \leq k_y \leq 8\,[\mathrm{cm}^{-1}]$ The experimental values in arbitrary units are scaled by a common factor.

C. Turbulence electron density spectra

The knowledge of the power-law spectra of a physical quantity is important for the understanding of the underlying physics and useful for providing constraints for simple physical models. Based on Kolmogorov-type arguments[28], turbulence is generally associated with universal power-law spectra. However, as shown in Refs 18, 29, and 30, this is generally not the case in plasma turbulence, and different power-law spectra indices can be found depending on the type of mechanism which drives or dissipates energy in the system.

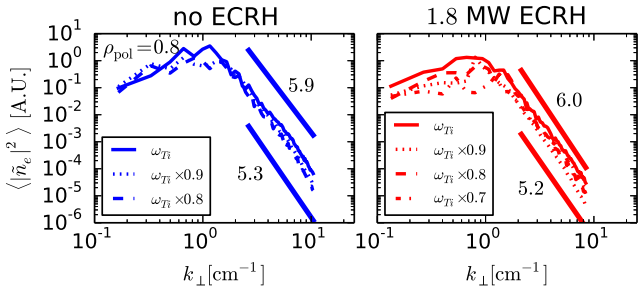

FIG. 7. (color online) Electron density fluctuations spectra at $\rho_{\mathrm{pol}} = 0.8$ including the variation of the logarithmic ion temperature gradient. The solid lines represent the wavenumber range where the fit to a power law was done. Spectral indices for the flattest and steepest spectra are also indicated in the figure for each case.

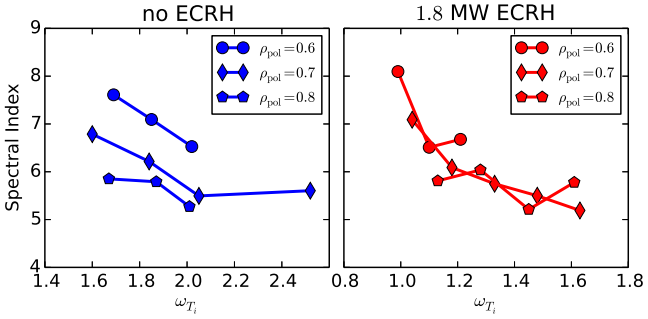

FIG. 8. (color online) Calculated spectral indices versus the logarithmic ion temperature gradient for different radial positions and ECRH scenarios. A decrease of the spectral indices with respect to the ion temperature gradient is observed for most of the cases.

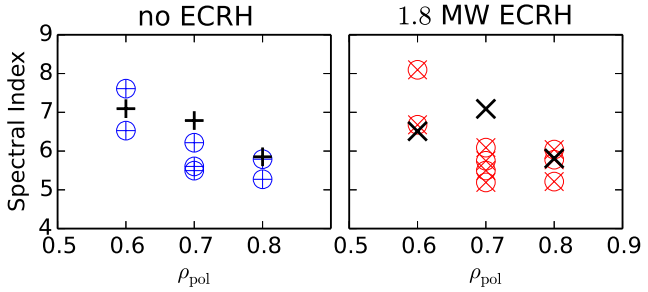

FIG. 9. (color online) Calculated spectral indices versus the radial position. Blue-plus markers represent the data without ECRH heating and red-cross markers with ECRH. The flux-match simulations are marked differently. A decrease of the spectral indices with respect to the radial position is observed.

Furthermore, the knowledge of wavenumber spectra could be important for a clear identification of the turbulent regimes driven by different microinstabilities and can be used to further validation of the gyrokinetic model.

The results of the electron density fluctuation spectra at $\rho_{\mathrm{pol}} = 0.8$ for different logarithmic ion temperature gradients are shown in Fig. 7. The solid lines represent the wavenumber range where a fit to a power law is shown: $\langle|\tilde{n}_e|^2\rangle = a\,k_\perp^{-b}$,

where b is the spectral index, and $\langle\rangle$ represents an average over all the coordinates except $k_\perp$. Spectral indices for the flattest and steepest spectra are indicated in the figure. The calculated spectral indices are also shown in Figs. 8 and 9 with respect to the ion temperature gradient and to the radial position, respectively. These figures present a clear qualitative behavior: the spectral index decreases with the increase of turbulence drive. Additionally, the spectral indices also decrease when going from the inner to the outer core position. Moreover, the magnitude of the exponents cover a wide range of values, approximately from 4 to 9. Although density fluctuation spectra were not measured with the Doppler reflectometer for this discharge, a similar trend has been also reported in Ref. 31 for various ASDEX Upgrade discharges.

These results indicate that the turbulence driven by ITG modes exhibits non-universal power laws, whose spectral indices could depend on several physical parameters. Future work in this respect will be to study also if TEM modes exhibit similar properties. If this was the case, then it would become very difficult to distinguish a type of instability by measuring only its characteristic spectral index.

D. Turbulence electron temperature amplitudes

At the time the discharge was performed, no temperature fluctuation measurements were available. However, a Correlation Electron Cyclotron Emission (CECE) diagnostic is currently installed on ASDEX Upgrade, and electron temperature fluctuation profiles will be available in the future campaigns.

The CECE diagnostic measures perpendicular electron temperature fluctuations ($\tilde{T}_{\perp,e}$) in the long wavelength range (relevant for ITG and TEM modes) and is not sensitive short wavelengths (ETG modes). This diagnostic presents an inherent limitation in the lowest fluctuation level that can be detected. This noise level depends on the physical parameters of the discharge, but typical values are between $0.2 - 0.3\,\%$[1].

A detailed description of CECE modeling in DIII-D is given in Ref. 32. This synthetic diagnostic has already been implemented in GENE for DIII-D discharges[6] and a similar synthetic diagnostic will be implemented for ASDEX Upgrade discharges. However, this diagnostic could be not used in this work since it requires the knowledge of the CECE configuration during the discharge. For this reason, we have considered a simpler synthetic diagnostic, which consists in filtering the gyrokinetic data to the positions and wavenumbers that are expected to be measured in ASDEX Upgrade. Consequently, the gyrokinetic data analysis results are restricted to the outboard mid-plane position ($z = 0$), averaged over the finite radial length and summing all perpendicular wavenumbers (since short wavelengths are not simulated). In order to better model the actual diagnostic, one should also apply a filter in the frequency space. However, this filter will also depend on the specific range of frequencies measured. Since we do not have access to this information, we have considered all the frequencies in the analysis. Therefore, the following results should be only used as an approximated indication of the fluctuation amplitudes that could be detected with CECE for this discharge. Nevertheless, we do not expect radial trends to change with respect to a more sophisticated synthetic diagnostic approach and only the amplitudes are likely to be rescaled[33].

The main results are shown in Fig. 10. The perpendicular electron temperature fluctuation amplitudes go from a minimum of $0.1\,\%$ at the inner position to a maximum of $1.0\,\%$ at the outer core position. Therefore, assuming a noise-level in the order of $0.2 - 0.3\,\%$ for the CECE diagnostic, this could imply that only the fluctuations at the outer core positions (starting from $\rho_{\rm pol} \geq 0.6$) could be detected. As for the case of the density amplitudes, we also observe a large variation of the fluctuation amplitudes with respect to the changes in the logarithmic ion temperature gradient.

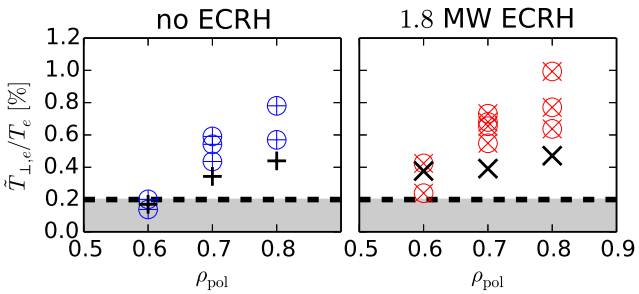

FIG. 10. (color online) Percentages of electron perpendicular temperature fluctuation amplitudes at different radial positions. Blue-plus markers represent the data without ECRH heating and red-cross markers with ECRH. The flux-match simulations are marked differently. The area shaded in grey indicates a typical noise level of the CECE diagnostic.

E. Turbulence cross-phases

Doppler reflectometers can be coupled to the CECE diagnostics to calculate cross-phases between electron density and temperature fluctuations[34]. This measurement is important for gyrokinetic validation studies since it represents a relationship between different fluctuating quantities (density and temperature in this case). In addition, this cross-phase could be also related to the cross-phase that determines the turbulent heat fluxes (electrostatic potential and temperature fluctuations). For this reason, in addition to the cross-phase that can be measured experimentally, we will also show the cross-phase between electrostatic potential and electron density fluctuations, so we can relate the cross-phases measured experimentally to the turbulent heat fluxes. The cross-phases are here defined as

$$\delta_{A,B} = \tan^{-1}\frac{\mathrm{Im}(A/B)}{\mathrm{Re}(A/B)}, \qquad (1)$$

for two observables A and B which are Fourier transformed in wave-number space.

Fig. 11 shows the variation of the cross-phase versus the ion temperature gradient integrated over binormal wavenumbers in the range of $1\,\mathrm{cm}^{-1} \leq k_y \leq 10\,\mathrm{cm}^{-1}$. For most of

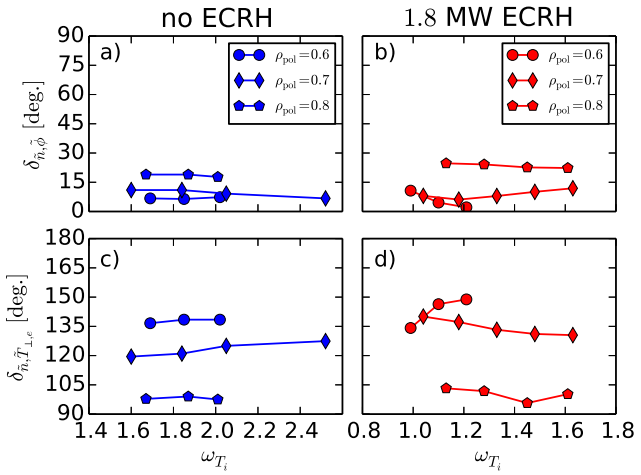

FIG. 11. (color online) Calculated cross-phases for the different cases versus the logarithmic ion temperature gradient. Cross-phases between density and electrostatic potential fluctuations (a) and (b). Cross-phases between electron density and temperature fluctuations (c) and (d). The cross-phases seem to be rather insensitive with respect to changes in the logarithmic ion temperature gradients.

the cases, the phases remain rather invariant with respect to the variation of this parameter. Therefore, this result seems to indicate that the cross-phase is a better observable to identify the type of instability which drives the turbulence in experiments, since TEM instability is expected to exhibit different cross-phases[35].

In Fig. 12, the cross-phase are displayed versus the radial positions. Regarding the cross-phase between density and electrostatic potential fluctuations (a) and (b), we see that they are practically in phase, i.e. close to 0. In addition, an increase of the phase with the radial position is also observed, going from practically 0 degrees at $\rho_{\rm pol} = 0.6$ to approximately 25 degrees at the outer core position. On the contrary, for the cross-phase between electron density and temperature fluctuations (c) and (d), we see a decrease with the radial position, going from around 150 degrees in the inner position to a value of 90 degrees, which result in an increase of the electron heat flux. Similar values of this cross-phase have also been measured in DIII-D and calculated with GYRO in Ref. 36. Furthermore, these values have also been found by GENE for these discharges, see Ref. 6. These observations could be explained in the following way. In the inner position, the population of the trapped particles that contributes to the ITG instability is small, so the electrons behave almost adiabatically. Because of this, density and potential fluctuations are in phase and density and perpendicular temperature fluctuations are almost out of phase (i.e., close to 90 degrees), thus producing negligible electron heat flux. With increasing the radial position, the population of trapped particles increase and a deviation of the electron adiabaticity is observed. For this reasons, both cross-phases approach to 90 degrees, with the subsequent increase of electron heat flux.

Finally, in Fig. 13, the colored contours display the cross-phases obtained from the nonlinear simulations, while the red squares are used to display the cross-phases of the linear simulations for the case without ECRH at $\rho_{\rm pol} = 0.6$. The agreement between linear and nonlinear cross-phases is remarkably good. This is also observed for the other cases[6,11,35]. This result implies that linear simulations could be enough to compare with experimental results.

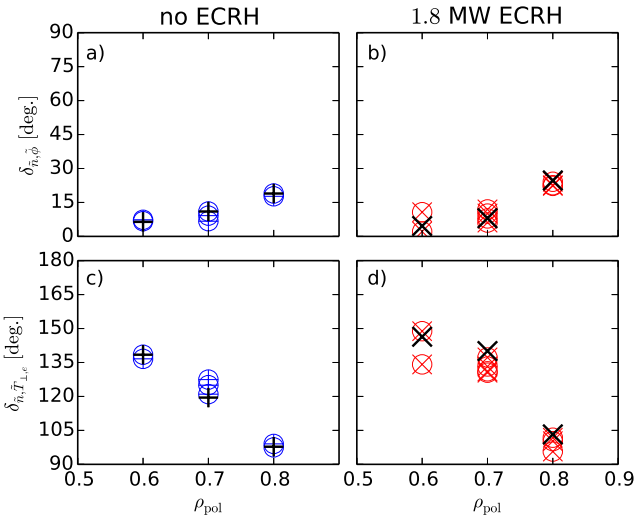

FIG. 12. (color online) Calculated cross-phases versus the radial position. Cross-phases between density and electrostatic potential fluctuations (a) and (b). Cross-phases between electron density and temperature fluctuations (c) and (d). The flux-match simulations are marked differently.

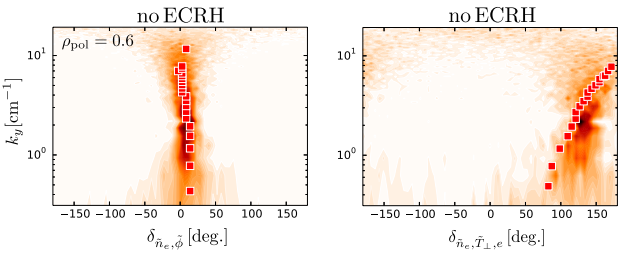

FIG. 13. (color online) Case without ECRH at $\rho_{\rm pol} = 0.6$: Comparison of linear (markers) and nonlinear (contour) cross-phases as function of the binormal wavenumber where amplitudes increase from white to black. Left. Cross-phases between electron density and electrostatic potential fluctuations. Right. Cross-phases between density and temperature fluctuations.

VI. DISCUSSION

Focusing on the case at $\rho_{\rm pol} = 0.7$ with 1.8 MW ECRH, the key results obtained in this paper can be illustrated in Fig. 14. Here, we show the impact of the variation of the logarithmic ion temperature gradient around the nominal value on various observables. Ion and electron heat fluxes (a), electron and temperature fluctuation amplitudes (b) and electron density spectral indices (c) are all very sensitive with respect

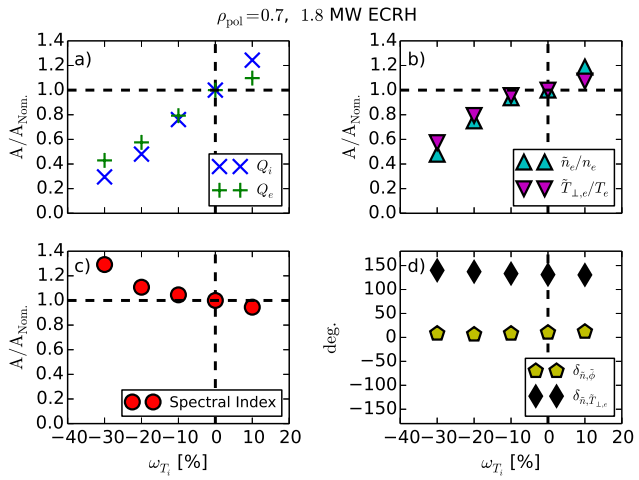

FIG. 14. (color online) Impact of the variation of the logarithmic ion temperature gradient around the nominal value for the case at $\rho_{\rm pol=0.7}$ with 1.8 MW ECRH on a) ion and electron heat fluxes b) electron density and temperature fluctuation amplitudes, c) electron density spectral index and d) cross phases. Figures a), b) and c) are normalized with respect to the value at the nominal ion temperature gradient.

to small changes in the ion logarithmic temperature gradient. For instance, by decreasing ω_{T_i} by 30%, the amplitudes can be reduced by a factor of 2 for the density and temperature fluctuations and by a factor of 4 for the heat fluxes. This result implies that the comparison of gyrokinetic simulation and experimental measurements for these observables are very sensitive to uncertainties in the experimental input profiles. On the contrary, cross-phases between density and temperature fluctuations and between density and electrostatic potential (d) are rather insensitive with respect to ω_{T_i}. This, together with the fact that linear and nonlinear cross-phases agreed also remarkably well, indicates that cross-phases could be a good observable to compare (fast) linear gyrokinetic simulations with experimental measurements.

VII. CONCLUSIONS AND FUTURE WORK

We have analyzed, by means of gyrokinetic simulations with GENE, core turbulence features of an H-mode discharge in ASDEX Upgrade. The main results of this paper can be summarized as follows. Flux-matched simulations were achieved by varying the nominal ion temperature gradient by a factor of $20-30\%$, which is within the uncertainty range of the experimental profiles. In addition, density fluctuation levels show an agreement in the shape of the radial turbulence level profiles, although the effect of the ECRH on the fluctuation levels was not reproduced. Non-universal power-law spectra were found for turbulence driven by ITG modes. In particular, ITG instability exhibits spectral indices for the density fluctuation spectra which cover a broad range of values. These values depend on the radial position and also on the specific ion temperature gradient. Gyrokinetic simulations predict a decrease of the exponents with respect to both the increase of the ion temperature gradient and the increase of the radial position. These results could help validate future analytical theories and are useful for comparisons with other gyrokinetic codes and future measurements. Regarding the electron temperature fluctuations, we observe for the inner position ($\rho_{\rm pol}=0.6$) fluctuation amplitudes which are close to the sensitivity of the CECE diagnostic. Therefore, it is possible that only measurements at positions larger than $\rho_{\rm pol}=0.6$ could be detected with this diagnostic in such discharges. We hope that these results can provide guidance for the development of the CECE diagnostic that is currently being installed in ASDEX Upgrade. Finally, by analyzing cross-phases between density and temperature fluctuations and between density and electrostatic potential, we observed that linear and nonlinear cross-phases agree remarkably well, and that they are rather insensitive with respect to the variation of the ion temperature gradient, indicating that cross-phases could be a good observable with experimental measurements for comparisons.

For future work, GENE and ASDEX Upgrade comparisons will continue with the study of similar H-modes plasmas but with higher ECRH power (up to 3.6 MW). These discharges are expected to have peaked electron temperature profiles and allow TEM modes to be dominant. This will allow us to study fundamental differences between ITG and TEM modes from a microscopic level. Furthermore, additionally dedicated discharges have already been conducted in which detailed wavenumber spectra have been measured with the Doppler reflectometer. These comparisons, along with the inclusion of future CECE measurements, will help in further validating gyrokinetic codes and the development of synthetic diagnostics.

ACKNOWLEDGEMENTS

The authors would like to thank A. E. White, F. Ryter, G. D. Conway and U. Stroth for fruitful discussions. The simulations presented in this work were carried out using the HELIOS supercomputer system at the Computational Simulation Centre of International Fusion Energy Research Centre (IFERC-CSC), Aomori, Japan, and the HYDRA supercomputer at the Rechenzentrum Garching (RZG), Germany. This work has been carried out within the framework of the EUROfusion Consortium and has received funding from the Euratom research and training programme 2014-2018 under grant agreement No 633053. The views and opinions expressed herein do not necessarily reflect those of the European Commission. The research leading to these results has also received funding from the European Research Council under the European Unions Seventh Framework Programme (FP7/2007V2013)/ERC Grant Agreement No. 277870.

[1] A. E. White, L. Schmitz, G. R. McKee, C. Holland, W. A. Peebles, T. A. Carter, M. W. Shafer, M. E. Austin, K. H. Burrell, J. Candy, J. C. DeBoo, E. J. Doyle, M. A. Makowski, R. Prater, T. L. Rhodes, G. M. Staebler, G. R. Tynan, R. E. Waltz, and G. Wang, *Phys. Plasmas* **17**, 056116 (2008).

[2]J. C. DeBoo, C. Holland, T. L. Rhodes, L. Schmitz, G. Wang, A. E. White, M. E. Austin, E. J. Doyle, J. C. Hillesheim, W. A. Peebles, C. C. Petty, Z.Yang, and L. Zeng, *Phys. Plasmas* **17**, 056105 (2010).
[3]C. Holland, L. Schmitz, T. L. Rhodes, W. A. Peebles, J. C. Hillesheim, G. Wang, L. Zeng, E. J. Doyle, S. P. Smith, R. Prater, K. H. Burrell, J. Candy, R. E. Waltz, J. E. Kinsey, G. M. Staebler, J. C. DeBoo, C. C. Petty, G. R. McKee, Z. Yan and A. E. White, *Phys. Plasmas* **18**, 056113 (2011).
[4]C. Holland, J. C. DeBoo, T. L. Rhodes, L. Schmitz, J. C. Hillesheim, G. Wang, A. E. White, M. E. Austin and E. J. Doyle, W. A. Peebles, C. C. Petty, L. Zeng and J. Candy, *Nuclear Fusion*, **52**, 063028 (2012).
[5]C. Holland, J. E. Kinsey, J. C. DeBoo, K. H. Burrell, T. C. Luce, S. P. Smith, C. C. Petty, A. E. White, T. L. Rhodes, L. Schmitz, E. J. Doyle, J. C. Hillesheim, G. R. McKee6, Z. Yan, G. Wang, L. Zeng, B. A. Grierson, A. Marinoni, P. Mantica, P. B. Snyder, R. E. Waltz, G. M. Staebler and J. Candy, *Nuclear Fusion*, **53**, 083027 (2013).
[6]T. Görler, A. E. White, D. Told, F. Jenko, C. Holland, and T. L. Rhodes, *Phys. Plasmas* **21**, 122307 (2014).
[7]A. E. White, N. T. Howard, M. Greenwald, M. L. Reinke, C. Sung, S. Baek, M. Barnes, J. Candy, A. Dominguez, D. Ernst, C. Gao, A. E. Hubbard, J. W. Hughes, Y. Lin, D. Mikkelsen, F. Parra, M. Porkolab, J. E. Rice, J. Walk, S. J. Wukitch, and Team Alcator C-Mod, *Phys. Plasmas* **20**, 056106 (2013).
[8]A. Casati, T. Gerbaud, P. Hennequin, C. Bourdelle, J. Candy, F. Clairet, X. Garbet, V. Grandgirard, Ö. Gürcan, S. Heuraux, G. T. Hoang, C. Honoré, F. Imbeaux, R. Sabot, Y. Sarazin, L. Vermare, and R. E. Waltz, *Phys. Rev. Lett.* **102**, 165005 (2009).
[9]S. Leerink, V. V. Bulanin, A. D. Gurchenko, E. Z. Gusakov, J. A. Heikkinen, S. J. Janhunen, S. I. Lashkul, A. B. Altukhov, L. A. Esipov, M. Yu. Kantor, T. P. Kiviniemi, T. Korpilo, D. V. Kuprienko, A. V. Petrov, *Phys. Rev. Lett.* **109**, 165001 (2012).
[10]T. Happel, A. Bañón Navarro, G. D. Conway, C. Angioni, M. Bernert, M. Dunne, E. Fable, B. Geiger, T. Görler, F. Jenko, R. M. McDermott, F. Ryter, U. Stroth and the ASDEX Upgrade Team, *Phys. Plasmas* **22**, 032503 (2015).
[11]D. Told, F. Jenko, T. Görler, F. J. Casson, E. Fable and the ASDEX Upgrade Team, *Phys. Plasmas* **20**, 122312 (2013).
[12]F. L. Hinton, and R. D. Hazeltine, *Rev. Mod. Phys.* **48**, 239 (1976).
[13]F. Jenko, W. Dorland, M. Kotschenreuther, and B. N. Rogers, *Phys. Plasmas*, **7**, 1904 (2000); see also: http://gene.rzg.mpg.de.
[14]H. Doerk, Ph.D. Dissertation, Universität Ulm (2013).
[15]P. Xanthopoulos, W. A. Cooper, F. Jenko, Yu. Turkin, A. Runov, and J. Geiger, *Phys. Plasmas*, **16**, 2303 (2009).
[16]P. Morel, A. Bañón Navarro, M. Albrecht-Marc, D. Carati, F. Merz, T. Görler and F. Jenko, *Phys. Plasmas* **18**, 072301 (2011).
[17]P. Morel, A. Bañón Navarro, M. Albrecht-Marc, D. Carati, F. Merz, T. Görler and F. Jenko, *Phys. Plasmas* **20**, 022501 (2013).
[18]A. Bañón Navarro, B. Teaca, F. Jenko, G. W. Hammet and T. Happel *Phys. Plasmas* **21**, 032304 (2014).
[19]In Ref. 10, the gradients are given in terms of the major radius in opposite to the reference length (proportional to the minor radius) used in this paper, see Table I for the specific values.
[20]T. Görler and F. Jenko, *Phys. Rev. Lett.* **100**, 185002 (2008).
[21]T. Görler and F. Jenko, *Phys. Plasmas* **15**, 102508 (2008).
[22]N. T. Howard, A. E. White, M. Greenwald, M. L. Reinke, J. Walk, C. Holland, J. Candy, and T. Görler, *Phys. Plasmas* **20**, 032510 (2013).
[23]N. T. Howard, A. E. White, M. L. Reinke, M. Greenwald, C. Holland, J. Candy, and J. R. Walk, *Nucl. Fusion* **53**, 123011 (2013).
[24]R. L. Miller, M. S. Chu, J. M. Greene, Y. R. Lin-Liu, and R. E. Waltz, *Phys. Plasmas* **5**, 973 (1998).
[25]G. Pereverzev and P. N. Yushmanov, Technical Report No. IPP 5/98, Max-Planck Institute (unpublished).
[26]J. C. Hillesheim, C. Holland, L. Schmitz, S. Kubota, T. L. Rhodes, and T. A. Carter, *Review of Scientific Instruments* **83**, 10E331 (2012).
[27]C. Lechte, G. D. Conway, T. Görler, C. Tröster, and the ASDEX Upgrade Team, 41st EPS Conference on Plasma Physics.
[28]G. Falkovich and K.R. Sreenivasan, Physics Today **59**, 43 (2006).
[29]V. Bratanov, F. Jenko, D. R. Hatch, and M. Wilczek, *Phys. Rev. Lett.* **111**, 075001 (2013).
[30]S. .S. Cerri, A. Bañón Navarro, F. Jenko, and D. Told, *Phys. Plasmas* **21**, 082305 (2014).
[31]C. H. Tröster, Ph.D thesis. Ludwig-Maximilians-Universität, München.
[32]M. W. Shafer, R. J. Fonck, G. R. McKee, C. Holland, A. E. White, and D. J. Schlossberg, *Phys. Plasmas* **19**, 032504 (2012).
[33]C. Holland, A. E. White, G. R. McKee, M. W. Shafer, J. Candy, R. E. Waltz, L. Schmitz, and G. R. Tynan *Phys. Plasmas* **16**, 052301 (2009).
[34]J. C. Hillesheim, J. C. DeBoo, W. A. Peebles, T. A. Carter, G. Wang, T. L. Rhodes, L. Schmitz, G. R. McKee, Z. Yan, G. M. Staebler, K. H. Burrell, E. J. Doyle, C. Holland, C. C. Petty, S. P. Smith, A. E. White, and L. Zeng, *Phys. Rev. Lett.* **110**, 045003 (2013).
[35]T. Dannert, and F. Jenko, *Phys. Plasmas* **12**, 072309 (2005).
[36]A. E. White, L. Schmitz, W. A. Peebles, T. L. Rhodes, T. A. Carter, G. R. McKee, M. W. Shafer, G. M. Staebler, K. H. Burrell, J. C. DeBoo, and R. Prater, *Phys. Plasmas* **17**, 020701 (2010).